

# Colossal orbital-Edelstein effect in non-centrosymmetric superconductors

Luca Chirolli,<sup>1,2</sup> Maria Teresa Mercaldo,<sup>3</sup> Claudio Guarcello,<sup>3</sup> Francesco Giazotto,<sup>2</sup> and Mario Cuoco<sup>4,3</sup>

<sup>1</sup>*Department of Physics, University of California, Berkeley, CA-94720*

<sup>2</sup>*NEST, Istituto Nanoscienze-CNR and Scuola Normale Superiore, Piazza San Silvestro 12, I-56127 Pisa, Italy*

<sup>3</sup>*Dipartimento di Fisica “E. R. Caianiello”, Università di Salerno, IT-84084 Fisciano (SA), Italy*

<sup>4</sup>*SPIN-CNR, IT-84084 Fisciano (SA), Italy*

In superconductors that lack inversion symmetry, the flow of supercurrent can induce a non-vanishing magnetization, a phenomenon which is at the heart of non-dissipative magneto-electric effects, also known as Edelstein effects. For electrons carrying spin and orbital moments a question of fundamental relevance deals with the orbital nature of magneto-electric effects in conventional spin-singlet superconductors with Rashba coupling. Remarkably, we find that the supercurrent-induced orbital magnetization is more than one order of magnitude greater than that due to the spin, giving rise to a colossal magneto-electric effect. The induced orbital magnetization is shown to be sign tunable, with the sign change occurring for the Fermi level lying in proximity of avoiding crossing points in the Brillouin zone and in the presence of superconducting phase inhomogeneities, yielding domains with opposite orbital moment orientation. The orbital-dominated magneto-electric phenomena, hence, have clear-cut marks for detection both in the bulk and at the edge of the system and are expected to be a general feature of multi-orbital superconductors without inversion symmetry breaking.

*Introduction.*— The success in designing spintronic and spinorbitronic devices relies on effects to generate, manipulate and detect spin-polarized currents. The Rashba spin-orbit coupling [1, 2] has a special role in this context because it allows to directly tune the electron spin orientation through its propagation and, viceversa, to achieve a spin control of the electron trajectories [3], thus giving rise to a large variety of magneto-electric effects. The most notable manifestations are the spin Hall effect [4–7] as well as the direct and inverse Edelstein effects (EE and IEE) [8–10], with a magnetization being induced by an electric current or, conversely, a non-equilibrium magnetization leading to charge current, respectively.

Recently, it has been recognized that an effect akin to the spin-Rashba (SR) in two-dimensional electron systems (2DES) arises due to the coupling between the atomic orbital angular momentum  $\mathbf{L}$  and the crystal wave-vector  $\mathbf{k}$  [11–14]. For materials having electronic states with non-vanishing  $\mathbf{L}$  close to the Fermi level, an intrinsic crystalline potential or an applied electric field that break spatial inversion can yield non-local odd-parity matrix elements among distinct atomic orbitals. The resulting orbital Rashba effect (ORE) [11–14], in analogy with the spin Rashba effect (SRE), confers chirality to the electronic states at the Fermi level, that acquire a momentum-dependent orbital texture [13–17].

Orbital physics can then give rise to orbital analogue phenomena of the spin Hall and spin Edelstein effects, namely orbital Hall [18–20] and orbital Edelstein effects [21–24], with the latter leading to a current-induced orbital magnetization. Brought into the context of non-dissipative superconducting magnetoelectric effects, so far the focus has been mostly on the spin degrees of freedom for spin-Rashba type superconductors [25–30] in-

cluding the generalization to all gyrotropic crystal point groups [31]. However, since electrons carry both spin and orbital moments, assessing the role of electrons’ orbital moment in setting out the magneto-electric effects is of fundamental relevance.

In this manuscript, we study the emergence of magneto-electric effects induced by a supercurrent flow in 2D non-centrosymmetric superconductors featuring an orbital Rashba (OR) coupling. We show that the supercurrent-induced orbital moments can exhibit striking marks with an extraordinary large amplitude and sign tunability. We find that the strength of the orbital polarization is more than one order of magnitude greater than that due to the spin, for nominally equal Rashba coupling strength. This colossal effect is then general, irrespective of the intensity of the OR coupling compared to the Fermi energy. The orbital Edelstein effect becomes particularly enhanced for the Fermi level lying in proximity of avoiding crossing points in the band structure induced by the orbital Rashba coupling, where it also features a sign change. The orientation of the induced orbital magnetization can be suitably tuned by sweeping the Fermi level across the avoided crossing, providing a knob to master the response. The sign change occurs not only for uniform configurations but also in the presence of superconducting phase inhomogeneities thus providing a route to devise domains with opposite magnetization. We discuss direct experimental probes of the effect and the impact that an applied electric field can have in guiding the suppression of the superconducting state by orbital magneto-electric effects.

*Model.*— In order to directly evaluate the contribution due to the electrons’ orbital moment and compare it with the spin one, we consider a 2D electronic system that explicitly includes the spin or orbital Rashba couplings. For

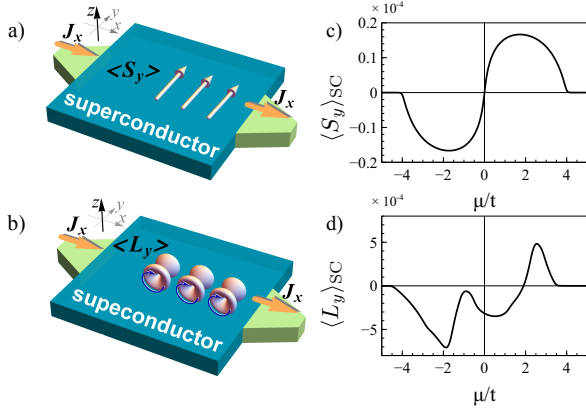


FIG. 1. Schematic setup showing the Edelstein effect in (a) spin- and (b) orbital- Rashba 2D systems with a supercurrent  $J_x$  flowing along the  $x$ -axis and the corresponding induced magnetization in the transverse  $y$ -direction. Induced (c) spin- and (d) orbital-polarization integrated in the whole Brillouin zone for a 2D Rashba system as a function of the chemical potential for  $\alpha = 0.1t$  and  $q = 0.02$  in unit of the inverse atomic distance. The maximum of the induced orbital moment  $\langle L_y \rangle$  is about 60 times larger than the corresponding spin polarization  $\langle S_y \rangle$  for the same amplitude of the Rashba coupling. In (d) the employed parameters are  $t' = 0.4t$  and  $\delta_z = 0.5t$ .

the OR case, the minimal description is based on three bands arising from atomic orbitals spanning the  $L = 1$  angular momentum subspace. This model applies for  $p$  orbitals or  $d$  orbitals, e.g.  $\{d_{yz}, d_{xz}, d_{xy}\}$ . As several materials can be effectively described with similar multi-orbital degrees of freedom close to the Fermi level, we keep the analysis general and refer for simplicity to  $d_a$  orbitals, with  $a = (yz, xz, xy)$ , at each site assuming a square lattice characterized by  $C_{4v}$  point group symmetry. The breaking of mirror symmetry, due to intrinsic crystalline potential or externally applied electric field, sets out a polar axis ( $z$ ) resulting into an orbital Rashba interaction that couples the atomic angular momentum  $\mathbf{L}$  with the crystal wave-vector  $\mathbf{k}$ . The Hamiltonian in momentum space is generally written as

$$h_0(\mathbf{k}) = \sum_a \epsilon_a(\mathbf{k}) \mathbb{P}_a + \alpha (\mathbf{g}_{\mathbf{k}} \wedge \hat{\mathbf{L}}) \cdot \hat{\mathbf{z}} - \mu, \quad (1)$$

where  $\epsilon_a(\mathbf{k}) = -2t_a^x \cos(k_x) - 2t_a^y \cos(k_y) - \delta_a$  are dispersion relations resulting from symmetry-allowed nearest-neighbor hopping amplitudes, where  $t_{yz}^y = t_{xz}^x = t_{xy}^x = t_{xy}^y = t$ ,  $t_{yz}^x = t_{xz}^y = t'$ , and  $\mathbb{P}_a = (\hat{L}^2 - \hat{L}_a^2)/2$  is a projector on the orbital  $a$  subspace. At the  $\Gamma$  point a degeneracy occurs between, say, the  $xz$  and the  $yz$  orbitals, thus for convenience we set  $\delta_{xz} = \delta_{yz} = 0$ . In turn, the orbital  $xy$  can show a finite crystal field splitting  $\delta_{xy} \equiv \delta_z$  that depends on the specific crystalline distortions.

The three bands are coupled at finite momentum by the orbital Rashba term described by a coupling constant

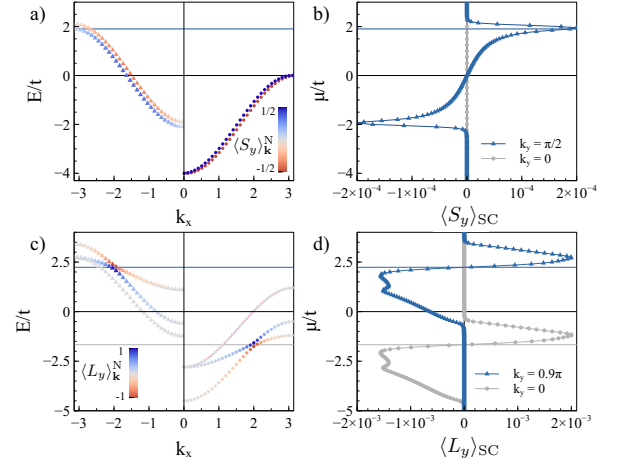


FIG. 2. (a) Spin-split Rashba bands for  $k_y = 0$  (plotted for positive  $k_x$ ) and  $k_y = \pi/2$  (for negative  $k_x$ ) for  $\alpha = 0.1t$ . The color map indicates the amplitude and sign of the  $k$ -resolved spin polarization in the normal state. (b) Induced spin-polarization for the spin-Rashba model in the superconducting state, as a function of the chemical potential  $\mu$  for two representative cuts in the Brillouin zone as shown in (a). (c) Cuts of the orbital-resolved band structure for  $\alpha = 0.1t$  at  $k_y = 0$  (positive  $k_x$ ) and at  $k_y = 0.9\pi$  (negative  $k_y$ ), respectively. The color map indicates the amplitude and sign of the  $k$ -resolved angular momentum polarization in the normal state. (d) Energy-resolved induced orbital moment in the superconducting state for the two cuts reported in (c). The sign change of the  $\langle L_y \rangle_{SC}$  occurs in proximity of the band touching at  $\mu/t \sim -1.67(2.24)$  for  $k_y = 0$  ( $k_y = 0.9\pi$ ), respectively. The employed parameters are  $t' = 0.4t$  and  $\delta_z = 0.5t$ .

$\alpha$  and involving the components of the angular momentum that in a matrix form are given by  $[\hat{L}_{\mathbf{k}}]_{lm} = i\epsilon_{klm}$  with  $\epsilon_{klm}$  the Levi-Civita tensor. Here, the OR coupling is specified by a vector  $\mathbf{g}(\mathbf{k}) = (\sin(k_x), \sin(k_y), 0)$  in momentum space that sets out the chirality of the orbital texture.

We now assume a finite chemical potential and a purely local ( $s$ -wave) attractive interaction of strength  $-U < 0$  leading to pairing of electrons with same orbital character. This gives rise to spin-singlet superconductivity described by a uniform gap  $\Delta = -U \langle \hat{d}_{a,\downarrow}(\mathbf{r}) \hat{d}_{a,\uparrow}(\mathbf{r}) \rangle$  on the Fermi surface, with  $\hat{d}_{a,s}(\mathbf{r})$  fermionic annihilation operators associated to  $d_a$  orbitals at position  $\mathbf{r}$  with spin  $s$ .

*Magnetization.*— The Edelstein effect in spin Rashba coupled superconductors manifests as a finite spin polarization in response to an applied supercurrent (Fig. 1(a)). The wedge product of polar vectors associated to the direction of the mirror symmetry breaking,  $\mathbf{z}$ , and the supercurrent  $\mathbf{J}$ , allows the construction of an axial vector

$$\mathbf{M} \sim \mathbf{z} \wedge \mathbf{J}, \quad (2)$$

and an in-plane spin magnetization, orthogonal to the applied bias current, is expected (Fig. 1(a)). As in the

SRE, an orbital moment develops on the Fermi surface and an analogous orbital Edelstein effect for the ORE is expected as in Fig. 1(c), with a finite orbital magnetization  $\mathbf{M} = \langle \mathbf{L} \rangle$  (in unit of the Bohr magneton  $\mu_B$ ).

In the presence of a current bias the order parameter acquires a position-dependent phase,  $\hat{\Delta}(\mathbf{r}) = \hat{\Delta}e^{i\mathbf{q}\cdot\mathbf{r}}$  for a finite  $\mathbf{q}$  sustained by the bias current. The phase bias can be absorbed in the fermionic operators  $\hat{d}_{a,s} \rightarrow \hat{d}_{a,s}e^{-i\mathbf{q}\cdot\mathbf{r}/2}$  through a gauge transformation and appears as a  $\mathbf{q}/2$  shift in momentum with opposite sign for particles and holes. For weak values of the applied current we can expand the magnetization at first order in the momentum  $\mathbf{q}$  and write the magnetization in linear response theory as

$$\langle \hat{L}_\mu \rangle = -\frac{1}{2}\chi_{\mu\nu}q_\nu, \quad (3)$$

with  $\chi_{\mu\nu}$  a static susceptibility between the angular momentum  $\hat{L}_\mu$  and the velocity operator defined as  $\hat{v}_\mu = \partial h_0 / \partial k_\mu$ , that is composed by a normal and an anomalous term and acquires no structure in particle-hole space. Thanks to the presence of a finite superconducting gap in the spectrum and the spontaneous breaking of U(1) symmetry, the static susceptibility can be obtained by energy correction at second-order perturbation theory and is essentially determined by the matrix elements  $v_x^{n,n'} L_y^{n',n} \equiv \langle \phi_{n,\mathbf{k}} | \hat{v}_x | \phi_{n',\mathbf{k}} \rangle \langle \phi_{n',\mathbf{k}} | \hat{L}_y | \phi_{n,\mathbf{k}} \rangle$ , with  $|\phi_{n,\mathbf{k}}\rangle$  eigenstates of  $h_0(\mathbf{k})$ , Eq. (1), with eigenvalues  $\epsilon_{n,\mathbf{k}}$ . Since we will consider separately the case of spin and orbital Rashba coupling, we use a unique coupling constant  $\alpha$  for both cases.

The comparison of the outcome of the total spin and orbital moments for the spin- and orbital-Rashba 2DES is reported in Fig. 1(b),(d). There are two striking features that can be immediately observed. The first one concerns with the amplitude of the effect. The evolution of the magnetization as a function of the electron filling, via a change in the chemical potential, shows that the induced orbital moment is generally much larger than the spin moment, with a maximum in the orbital channel that can be up to about 60 times bigger than the spin one, even for nominally equal coupling constant. The second relevant aspect is the sign tunability for values of the chemical potential that are in proximity of avoiding crossings at small transverse to the current momenta,  $k_y$ , in the electronic structure. The sign change of the total response for the ORE case (occurring at  $\mu/t \sim 1.8$  in Fig. 1 (d)) has its origin in the avoided crossings appearing in the band structure (Fig. 2 (c) and (d)). The latter occurs in generic points in the Brillouin zone because orbitals, differently from spin, are not forced to be degenerate at high symmetry point by Kramers' theorem, that guarantees spin degeneracy. In particular, the symmetry of the orbitals and the crystal point group of the material may allow a crystal field splitting to appear. The latter can then shift the avoided crossing at arbitrary energy,

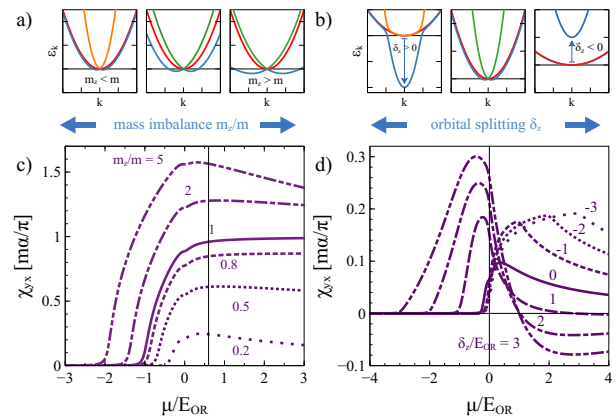


FIG. 3. Schematics of the evolution of the bands around the  $\Gamma$  point in the  $C_{\infty v}$  symmetry by varying a) the orbital mass imbalance  $m_z/m$  for  $\delta_z = 0$  and b) the crystal field splitting  $\delta_z$  for  $m_z = 5m$ . Edelstein susceptibility versus the chemical potential  $\mu$  in units of  $E_{OR} = m\alpha^2/2$  by varying c) the orbital mass ratio  $m_z/m$  for  $\delta_z = 0$  and d) the crystal field splitting  $\delta_z/E_{OR}$  for  $m_z = 5m$ .

resulting in orbital tunable magneto-electric effects not only in semi-metallic but also in metallic states. In turn, the sign change of the spin moment for the SRE is due to the sublattice symmetry of the tight-binding model at specific points in parameter space and manifests at  $\mu = 0$ .

A simple way to understand the different spin and orbital response of the system is to consider 1D cuts of the band structure by fixing the transverse momentum  $k_y$  (Fig. 2). In particular, for  $k_y = 0, \pi$ , one band in the orbital-Rashba case completely decouples. In this specific case, the matrix element appearing in the susceptibility (see Eq. (8) of Methods) reads

$$v_x^{+,-} L_y^{-,+} = \alpha(\epsilon_1 - \epsilon_2) \frac{(\epsilon_1 - \epsilon_2) \partial_x g_x - g_x (v_x^1 - v_x^2)}{4\alpha^2 g_x^2 + (\epsilon_1 - \epsilon_2)^2}, \quad (4)$$

with  $\partial_x \equiv \partial / \partial k_x$ ,  $\epsilon_{1(2)} = \epsilon_{yz(xz)}(k_x)$ , and  $v_{1(2)} = \partial_x \epsilon_{yz(xz)}(k_x)$ . Clearly, in the case of spin-Rashba, the unperturbed spin degenerate bands satisfy  $\epsilon_1 = \epsilon_2$  and the Edelstein susceptibility is exactly zero (Fig. 2(b)). In turn, the susceptibility for the orbital-Rashba case is non zero due to the difference in effective masses and crystal field splitting that characterize the dispersions originating from different orbitals. At finite momentum  $k_y$  the susceptibility in the spin-Rashba case becomes finite and allows a direct comparison of the response between the two cases. In Fig. 2(a) we show the bands at  $k_y = 0(\pi/2)$  for positive (negative)  $k_x$  of the spin-Rashba model for  $\alpha = 0.1t$  and in Fig. 2(b) the induced spin magnetization evaluated for  $q = 0.02$  (in units of the inverse atomic lattice constant). The linear response condition is satisfied and the magnetization is proportional to the applied momentum via the susceptibility. A finite response is found

for non-zero  $k_y$ , peaked at the band splitting nearby the  $\Gamma$  point.

The Edelstein magnetization for the case of the ORE is more interesting. In Fig. 2(c) we show the bands at  $k_y = 0(0.9\pi)$  for positive (negative)  $k_x$  of the orbital-Rashba model for  $t' = 0.4t$  and  $\alpha = 0.1t$ . A light effective mass band, originating from the  $d_{xy}$  orbital, detaches and shifts down in energy with respect to the other two bands originating from the  $d_{yz}$  and  $d_{xz}$  orbitals, that remain degenerate at the  $\Gamma$  point. As a result the light and heavy bands cross at finite momentum and an avoided crossing is generated at finite  $\alpha$ . This is generally expected to occur for 2DES. An additional crystal field splitting  $\delta_z = 0.5t$  is added to tune the avoided crossing position.

In Fig. 2(d) the induced orbital moment for  $q = 0.02$  is shown. The response is finite for every  $k_y$  and a sign change appears that is pinned to the avoided crossing. This is understood at  $k_y = 0$  by inspection of Eq. (4). At the avoided crossing,  $\epsilon_1 = \epsilon_2$  and the sign of the matrix element is determined by the velocity difference  $v_x^1 - v_x^2$ . As the two velocities interchange at the avoided crossing the magnetization features a sign change. Furthermore, as shown by the color code in Fig. 2(c), the expectation value of  $\hat{L}_y$  is maximal at the avoided crossing, yielding peaks above and below the sign change. By increasing  $k_y$ ,  $\hat{L}_y$  decreases in amplitude according to the structure of the orbital Rashba, and, due to the admixture with the third band a shift of the avoided crossing in energy occurs. The full response (Fig. 1(d)), integrated on all  $k_y$ 's, features a vanishing point in proximity of the highest in energy avoided crossing and its magnitude is about sixty times larger than in the spin-Rashba case.

*Orbital splitting and mass imbalance.* — As previously anticipated, one of the main difference between SR and OR cases is the absence of a Kramer's theorem that forces an orbital degeneracy at high symmetry points in the Brillouin zone. It follows that the Edelstein effect in the OR case shows a strong dependence on the effective masses and crystal field splittings in amplitude and sign. To simplify the analysis we expand the Hamiltonian around the  $\Gamma$  point, where the orbital Rashba term becomes invariant for any rotation about the  $z$  axis, and extend the  $C_{\infty v}$  symmetry to the effective masses. This way, the avoided crossing observed in Fig. 1 are now at the same energy for all  $k_x$  and  $k_y$  and the dependence of the Edelstein effect on effective masses and crystal field splitting becomes manifest. In turn, the Edelstein response for the SR case around the  $\Gamma$  point is featureless, with no sign change and a constant susceptibility for positive  $\mu$  that resembles the curve  $m = m_z$  in Fig. 3 (c).

In Fig. 3(a) we show the evolution of the bands by increasing or decreasing the ratio  $m_z/m$ . For  $m_z/m \neq 1$  two of the three bands tend to collapse on top of the other, so that their relative contribution vanishes and a partial cancellation of the contributions from different bands takes place. The susceptibility, shown in Fig. 3(c)

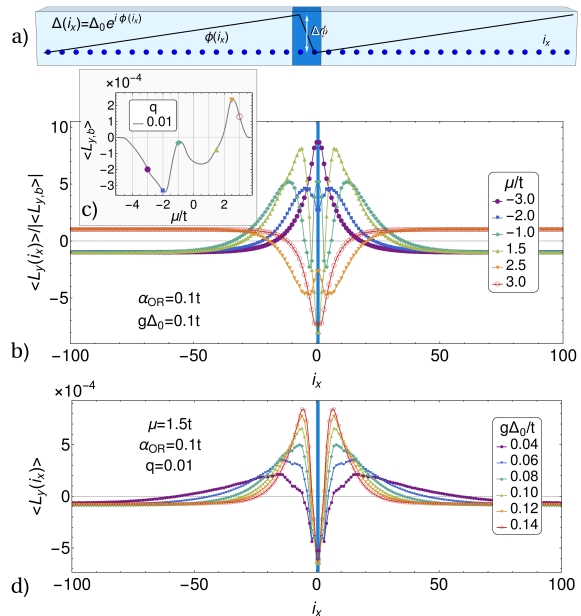


FIG. 4. (a) Sketch of the superconducting phase across the superconductor along a given direction in real space with a change of the phase gradient by  $\Delta\phi$  around the position  $i_x = 0$ . (b) Real space dependence of the orbital polarization renormalized to the bulk value  $\langle L_{y,b} \rangle$  reported in (c) for several values of the chemical potential. In proximity of the domain boundary ( $i_x = 0$ ) the orbital moment has an enhancement of the amplitude of about 10 times with respect to the bulk, and a sign change occurring at a distance of about the superconducting coherence length. (d) Plot of the spatial resolved orbital moment for a representative value of  $\mu$  and  $\alpha$  for different values of the superconducting order parameter  $\Delta_0$ . The increase of the gap amplitude induces a sign change of the orbital polarization at a shorter distance from the phase domain boundary thus scaling with the coherence length amplitude. The employed parameters are  $t' = 0.4t$ ,  $\delta_z = 0.5t$ , while the hopping amplitude at the domain boundary is  $t_b = 0.75t$ .

is dominated by the residual contribution, that is proportional to the difference in the Fermi momenta and in the case  $m_z/m > 1$  the signal increases.

In Fig. 3(b) we show the evolution of the bands by varying the value of the crystal field splitting  $\delta_z$  and we choose a large difference in the effective masses,  $m = 5m_z$ . This way, the band edge of the light mass band shifts down in energy for positive  $\delta_z$  and up in energy for negative  $\delta_z$ . An avoided crossing is then produced for positive  $\delta_z$ , as in the case illustrated in Fig. 2(c), and an interchange of the velocity above and below the avoided crossing produces a sign change in the susceptibility. The evolution from negative to positive  $\delta_z$  is shown in Fig. 3(d), and a clear sign change appears. We point out that the SRE case around the  $\Gamma$  point is featureless, showing no sign change and a constant susceptibility [30] resembling the  $m = m_z$  line in Fig. 3 (c).

*Spatial-dependent orbital Edelstein effects.* — The am-

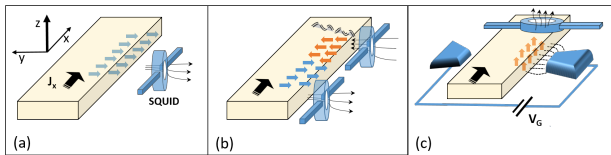


FIG. 5. Sketch of an experimental setup for the detection of the orbital moments generated by the supercurrent flow. We consider non-centrosymmetric or ultra-thin superconductors with  $z$  being the polar direction associated with inversion symmetry breaking. In the case of a uniform magnetization we expect that a magnetic flux along the direction of the orbital moment can be measured by SQUID along the lateral profile of the superconductor. (b) In presence of small phase inhomogeneities there is a reorientation of the orbital moments in real space that results into opposite fluxes along the lateral edge. (c) The application of an electric field with lateral split gates leads to an out-of-plane orbital polarization and in turn a magnetic flux that is oriented perpendicular to the surface of the superconductor.

plitude and sign of the ORE has also distinctive marks when considering its spatial dependence in the case of inhomogeneous superconducting phase profile. We have solved the orbital Rashba model (Eq. (1)) for a 2D system with size  $L_x \times L_y$ ,  $L_x = 200$ , in unit of the interatomic distance, and assuming translational invariance for  $L_y$ . The supercurrent profile includes a phase gradient in real space along a given direction (Fig. 4(a)) and a phase defect in the spatial profile of the supercurrent. Thus, we have a domain boundary with a weak modification of the phase gradient expressed by the variation  $\Delta\phi$  across the domain boundary at a given position. The aim here is to assess the spatial dependence of the induced orbital moment. The presence of a weak phase gradient change leads to two striking features. We find a general enhancement of the induced orbital moment (Fig. 4(b)) compared to the value in the bulk (Fig. 4(c)). Moreover, the orbital Edelstein effect exhibits a sign variation of the orbital moment in real space thus yielding domains with opposite orientation. The spatial extension of the domain with an amplification of the orbital polarization is of the order of the superconducting coherence length  $\xi_{SC}$ . We verify that for a ballistic superconductor, for which  $\xi_{SC} \sim v_F/\Delta$  with  $v_F$  the Fermi velocity, an increase of the gap amplitude leads to a reduction of the size of the region with enhanced orbital polarization (Fig. 4(d)).

*Discussion.*— The amplitude of the orbital contribution is extraordinary large if compared to that of the spin for nominally equal coupling constant  $\alpha$  and a colossal Edelstein response is demonstrated. Although similar in structure to the SRE, the origin of the ORE does not rely on the atomic spin-orbit interaction, instead it is solely due to a finite momentum-dependent overlap between Wannier orbitals enabled by the broken mirror symmetry. For this reason the magnitude of the OR coupling is typically much larger [32–36] than the

corresponding one in the spin channel. These features open the possibility to both a wide amplitude tunability of the Edelstein effect and sign variation through a gate that changes the charge density and allows us to sweep the Fermi level around avoided crossings. An ideal platform is represented by 2D superconductors realized at LAO/STO ( $\text{LaAlO}_3/\text{SrTiO}_3$ ) interfaces [37], where an electric field has been shown to be effective in varying the electron density and tuning the chemical potential close to orbitally driven avoided crossings [38]. Furthermore, since the disclosed orbital Edelstein effect requires solely s-wave superconductivity, its application can be extended to ultrathin elemental superconductors as well as hybrid implementations through proximized superconductivity.

Detection of the Edelstein effect can employ a SQUID (or other magnetic spectroscopic probes) since it is able to probe the spatial distribution of the magnetic field generated by the local magnetic moments, as depicted in Fig. 5 (a). The SQUID technique can directly give access to the dipolar field distribution with direction change occurring around phase defects or similar inhomogeneities, as depicted in Fig. 5 (b). Additionally, for inversion symmetry breaking generated via a side gate, as shown in Fig. 5 (c), an out-of-plane magnetic flux with the amplitude controlled by the electric field, is expected to be observed at the edge of the superconductor. The size of the induced local orbital moment can reach about  $10^{-4}\mu_B$ , and even higher by varying the OR coupling, which convert into dipolar fields of about hundred Gauss in close proximity of the 2DES. The dipolar field of the induced magnetization has a different spatial distribution compared to that due to the supercurrent especially in the presence of domains with opposite orbital moments, thus allowing a separate detection of the two contributions.

The Edelstein magnetization represents an explicitly time-reversal symmetry breaking perturbation, that, in turn, can have a non-trivial detrimental back action on the superconductor itself. A reduction of the critical current can result from the induced dipolar fields, especially when the size of the induced moment locally overcomes the critical magnetic fields. The supercurrent can thus be an optimal indicator in systems where an applied electric field varies the intensity of the Rashba coupling. We argue that the orbital Edelstein effect could have a non-trivial role in the suppression of critical current recently reported in experiments where an electric field is applied to metallic superconductors [39].

*Acknowledgments.*— L.C. acknowledges the European Commission for funding through the MSCA Global Fellowship grant TOPOCIRCUS-841894. M.C., M.T.M and F.G. acknowledge support by the EU’s Horizon 2020 research and innovation program under Grant Agreement nr. 964398 (SUPERGATE). F.G. acknowledges the European Research Council under Grant Agreement No. 899315-TERASEC, and the EU’s Horizon 2020 research and innovation program under Grant Agreement

No. 800923 (SUPERTED) for partial financial support.

### Methods.

BCS superconductivity is described by introducing the Nambu basis,  $\Psi^\dagger(\mathbf{r}) = (\hat{\mathbf{d}}_+^\dagger(\mathbf{r}), \hat{\mathbf{d}}_-^\dagger(\mathbf{r}))$ , with  $\hat{\mathbf{d}}_s(\mathbf{r})$  a column vector of annihilation Fermionic operators  $\hat{d}_{a,s}$  associated to the different orbitals. The mean-field Hamiltonian is then written as  $H = \int d\mathbf{r} \Psi^\dagger(\mathbf{r}) \mathcal{H}(\mathbf{r}) \Psi(\mathbf{r})$ , with  $\mathcal{H}(\mathbf{r})$  the Bogoliubov deGennes Hamiltonian featuring an explicit position dependence via the phase of the superconducting gap  $\Delta(\mathbf{r}) = \Delta e^{i\mathbf{q}\cdot\mathbf{r}}$ , with  $\mathbf{q}$  sustained by a finite bias current. Performing a gauge transformation on particle and hole states,  $\Psi(\mathbf{r}) \rightarrow e^{i\mathbf{q}\cdot\mathbf{r}\tau_z/2} \Psi(\mathbf{r})$ , we can map the position dependence of the gap in a momentum shift of opposite sign for particle and holes, so that the BdG Hamiltonian in momentum space takes the form

$$\mathcal{H}(\mathbf{k}, \mathbf{q}) = \begin{pmatrix} h_0(\mathbf{k} + \mathbf{q}/2) & \hat{\Delta}(\mathbf{q}) \\ \hat{\Delta}^\dagger(\mathbf{q}) & -h_0^*(-\mathbf{k} + \mathbf{q}/2) \end{pmatrix}, \quad (5)$$

where  $\hat{\Delta}(\mathbf{q})$  is a gap matrix proportional to the identity and we neglect the momentum dependence of the gap amplitude.

Following the same approach employed for the spin Rashba coupled superconductor, in the OR case the magnetization in response to an applied supercurrent is given by  $\langle \hat{L}_\mu \rangle = T \sum_{i\omega_n, \mathbf{k}} \text{Tr}[G_{i\omega_n}(\mathbf{k}, \mathbf{q}) \hat{L}_\mu]$ , where the Green's function in the Nambu space is given by  $-G_{i\omega_n}^{-1}(\mathbf{k}, \mathbf{q}) = -i\omega_n + \mathcal{H}(\mathbf{k}, \mathbf{q})$ . Expansion of the full Green's function at first order in  $\mathbf{q}$  yields the expression Eq. (3) in terms of a static susceptibility

$$\chi_{\mu\nu} = -T \sum_{i\omega_n, \mathbf{k}} \text{Tr} \left[ G_{i\omega_n}(\mathbf{k}) \hat{L}_\mu G_{i\omega_n}(\mathbf{k}) \hat{v}_\nu(\mathbf{k}) \right], \quad (6)$$

with the velocity operator is explicitly given by

$$\hat{v}_\mu(\mathbf{k}) = \sum_a \frac{\partial \epsilon_a(\mathbf{k})}{\partial k_\mu} \mathbb{P}_a + \alpha \hat{\mathbf{L}} \wedge \hat{z} \cdot \frac{\partial \mathbf{g}(\mathbf{k})}{\partial k_\mu}. \quad (7)$$

Assuming to apply the current bias along the  $x$  direction, the susceptibility can be written as

$$\chi_{yx} = 2 \sum_{\mathbf{k}, n > n'} \frac{1}{E_{n,\mathbf{k}} + E_{n',\mathbf{k}}} \left( 1 - \frac{\epsilon_{n,\mathbf{k}} \epsilon_{n',\mathbf{k}} + \Delta^2}{E_{n,\mathbf{k}} E_{n',\mathbf{k}}} \right) \times \text{Re} \langle \phi_{n,\mathbf{k}} | \hat{v}_x | \phi_{n',\mathbf{k}} \rangle \langle \phi_{n',\mathbf{k}} | \hat{L}_y | \phi_{n,\mathbf{k}} \rangle. \quad (8)$$

This expression is easily adapted to describe the Edelstein response in the spin-Rashba case by replacing the dispersion  $\epsilon_a(\mathbf{k})$  with degenerate bands, the angular momentum  $\hat{L}_\mu$  with spin Pauli matrices, and an overall factor 1/2 to avoid double counting spin-degeneracy. This way, a direct comparison between the two models can be made.

In the  $C_{v\infty}$  case around the  $\Gamma$  point the eigenvalues of the band Hamiltonian  $h_0$  have the general expression  $\epsilon_{0,k} = \epsilon_k$  and  $\epsilon_{\pm,k} = \epsilon_k + \delta\epsilon_{\pm,k}$ , with  $\delta\epsilon_{\pm,k} = (\epsilon_k^z - \epsilon_k \pm \sqrt{4k^2\alpha^2 + (\epsilon_k^z - \epsilon_k)^2})/2$ ,  $\epsilon_k^z = k^2/2m_z - \mu - \delta_z$ , and  $\epsilon_k = k^2/2m - \mu$ . The matrix elements that enter the susceptibility are then given by

$$\langle v_x^{0,\pm} L_y^{\pm,0} \rangle_\phi = \pm \frac{\alpha \delta \epsilon_\pm}{2(\epsilon_k^+ - \epsilon_k^-)}, \quad (9)$$

$$\langle v_x^{+,-} L_y^{-,+} \rangle_\phi = \frac{\alpha(\epsilon_k - \epsilon_k^z)}{(\epsilon_k^+ - \epsilon_k^-)^2} \left( \epsilon_k - \epsilon_k^z + \frac{\alpha k^2}{m_z} - \frac{\alpha k^2}{m} \right), \quad (10)$$

where  $\langle \dots \rangle_\phi$  denotes average over the azimuthal angle  $\phi = \tan^{-1}(k_y/k_x)$ . We see that  $\langle v_x^{+,-} L_y^{-,+} \rangle_\phi$  essentially agrees with Eq. (4).

- 
- [1] E. I. Rashba, *Properties of semiconductors with an extremum loop. I. Cyclotron and combinational Resonance in a magnetic field perpendicular to the plane of the loop*, Sov. Phys. Solid State **2**, 1109 (1960).
  - [2] G. Dresselhaus, *Spin-Orbit Coupling Effects in Zinc Blende Structures*, Phys. Rev. **100**, 580 (1955).
  - [3] A. Manchon, H. C. Koo, J. Nitta, S. M. Frolov, and R. A. Duine, *New perspectives for Rashba spin-orbit coupling*, Nat. Mater. **14**, 871 (2015).
  - [4] M. Dyakonov and V. Perel, *Current-induced spin orientation of electrons in semiconductors*, Phys. Lett. A **35**, 459 (1971).
  - [5] J. E. Hirsch, *Spin Hall Effect*, Phys. Rev. Lett. **83**, 1834 (1999).
  - [6] Y. K. Kato, R. C. Myers, A. C. Gossard, and D. D. Awschalom, *Observation of the spin Hall effect in semiconductors*, Science **306**, 1910 (2004).
  - [7] J. Sinova, S. O. Valenzuela, J. Wunderlich, C. H. Back, and T. Jungwirth, *Spin Hall Effects*, Rev. Mod. Phys. **87**, 1213 (2015).
  - [8] A. G. Aronov and Y. B. Lyanda-Geller, *Nuclear electric resonance and orientation of carrier spins by an electric field*, JETP Lett. **50**, 431 (1989).
  - [9] V. M. Edelstein, *Spin polarization of conduction electrons induced by electric current in two-dimensional asymmetric electron systems*, Solid State Commun. **73**, 233 (1990).
  - [10] K. Shen, G. Vignale, and R. Raimondi, *Microscopic Theory of the Inverse Edelstein Effect*, Phys. Rev. Lett. **112**, 096601 (2014).
  - [11] S. R. Park, C. H. Kim, J. Yu, J. H. Han, and C. Kim, *Orbital-angular-momentum based origin of Rashba-type surface band splitting*, Phys. Rev. Lett. **107**, 156803 (2011).
  - [12] J.-H. Park, C. H. Kim, J.-W. Rhim, and J. H. Han, *Orbital Rashba effect and its detection by circular dichroism angle-resolved photoemission spectroscopy*, Phys. Rev. B **85**, 195401 (2012).
  - [13] B. Kim, P. Kim, W. Jung, Y. Kim, Y. Koh, W. Kyung, J. Park, M. Matsunami, Shin-ichi Kimura, J. S. Kim, J. H. Han, and C. Kim, *Microscopic mechanism for asymmetric charge distribution in Rashba-type surface states*

- and the origin of the energy splitting scale, Phys. Rev. B **88**, 205408 (2013).
- [14] M. T. Mercaldo, P. Solinas, F. Giazotto, and M. Cuoco, *Electrically tunable superconductivity through surface orbital polarization*, Phys. Rev. Applied **14**, 034041 (2020).
- [15] J.-H. Park, C. H. Kim, H.-W. Lee, and J. H. Han, *Orbital chirality and Rashba interaction in magnetic bands*, Phys. Rev. B **87**, 041301(R) (2013).
- [16] B. Kim, C. H. Kim, P. Kim, W. Jung, Y. Kim, Y. Koh, M. Arita, K. Shimada, H. Namatame, M. Taniguchi, J. Yu, and C. Kim, *Spin and orbital angular momentum structure of Cu(111) and Au(111) surface states*, Phys. Rev. B **85**, 195402 (2012).
- [17] S. R. Park, J. Han, C. Kim, Y. Y. Koh, C. Kim, H. Lee, H. J. Choi, J. H. Han, K. D. Lee, N. J. Hur, M. Arita, K. Shimada, H. Namatame, and M. Taniguchi, *Chiral Orbital-Angular Momentum in the Surface States of  $Bi_2Se_3$* , Phys. Rev. Lett. **108**, 046805 (2012).
- [18] S. Zhang and Z. Yang, *Intrinsic Spin and Orbital Angular Momentum Hall Effect*, Phys. Rev. Lett. **94**, 066602 (2005).
- [19] T. Tanaka, H. Kontani, M. Naito, T. Naito, D. S. Hirashima, K. Yamada, and J. Inoue, *Intrinsic spin Hall effect and orbital Hall effect in 4d and 5d transition metals*, Phys. Rev. B **77**, 165117 (2008).
- [20] H. Kontani, T. Tanaka, D. S. Hirashima, K. Yamada, and J. Inoue, *Giant Intrinsic Spin and Orbital Hall Effects in  $Sr_2MO_4$  ( $M = Ru, Rh, Mo$ )*, Phys. Rev. Lett. **100**, 096601 (2008).
- [21] L. S. Levitov, Y. V. Nazarov, and G. M. Éliashberg, *Magneto-electric effects in conductors with mirror isomer symmetry*, Sov. Phys. JETP **61**, 133 (1985).
- [22] S. Zhong, J. E. Moore, I. Souza, *Gyrotropic Magnetic Effect and the Magnetic Moment on the Fermi Surface* Phys. Rev. Lett. **116**, 077201 (2-16).
- [23] L. Salemi, M. Berritta, A. K. Nandy, and P. M. Oppeneer, *Orbitally dominated Rashba-Edelstein effect in non-centrosymmetric antiferromagnets*, Nat. Comm. **10**, 5381 (2019).
- [24] A. Johannsson, B. Göbel, J. Henk, M. Bibes, and I. Mertig *Spin and orbital Edelstein effects in a two-dimensional electron gas: Theory and application to  $SrTiO_3$  interfaces*, Phys. Rev. Research **3**, 013275 (2021).
- [25] V. M. Edelstein, *Magnetoelectric effect in polar superconductors*, Phys. Rev. Lett. **75**, 2004 (1995).
- [26] V. M. Edelstein, *Magnetoelectric effect in dirty superconductors with broken mirror symmetry*, Phys. Rev. B **72**, 172501 (2005).
- [27] S. Yip, *Noncentrosymmetric superconductors*, Annu. Rev. Condens. Matter Phys., **5**, 15 (2014).
- [28] F. Korschelle, I. V. Tokatly, and F. S. Bergeret, *Theory of the spin-galvanic effect and the anomalous phase shift  $\phi_0$  in superconductors and Josephson junctions with intrinsic spin-orbit coupling*, Phys. Rev. B **92**, 125443 (2015).
- [29] I. V. Tokatly, *Usadel equation in the presence of intrinsic spin-orbit coupling: A unified theory of magnetoelectric effects in normal and superconducting systems*, Phys. Rev. B **96**, 060502(R) (2017).
- [30] J. J. He, K. Hiroki, K. Hamamoto, and N. Nagaosa, *Spin supercurrent in two-dimensional superconductors with Rashba spin-orbit interaction*, Commun. Physics **2**, 128 (2019).
- [31] W.-Y. He and K.T. Law, *Novel magnetoelectric effects in gyrotropic superconductors and a case study of transition metal dichalcogenides*, Phys. Rev. Research **2**, 012073 (2020).
- [32] D. Go, J.-P. Hanke, P. M. Buhl, F. Freimuth, G. Bihlmayer, H.-W. Lee, Y. Mokrousov, and S. Blügel, *Toward surface orbitronics: giant orbital magnetism from the orbital Rashba effect at the surface of sp-metals*, Sci. Rep. **7**, 46742 (2017).
- [33] T. Park, J. Hong, and J. H. Shim, *Enhancement of Giant Rashba Splitting in  $BiTeI$  under Asymmetric Inter-layer Interaction*, Journal of the Phys. Soc. of Japan **89**, 044701 (2020).
- [34] D. Go, D. Jo, T. Gao, K. Ando, S. Blügel, H.-W. Lee, and Y. Mokrousov, *Orbital Rashba effect in a surface-oxidized  $Cu$  film*, Phys. Rev. B **103**, L121113 (2021)
- [35] V. Sunko, H. Rosner, P. Kushwaha, S. Khim, F. Mazzola, L. Bawden, O. J. Clark, J. M. Riley, D. Kasinathan, M. W. Haverkort, T. K. Kim, M. Hoesch, J. Fujii, I. Vobornik, A. P. Mackenzie, and P. D. C. King, *Maximal Rashba-like spin splitting via kinetic-energy-coupled inversion-symmetry breaking*, Nature **549**, 492 (2017).
- [36] M. Ünzelmann, H. Bentmann, P. Eck, T. Kießlinger, B. Geldiyev, J. Rieger, S. Moser, R. C. Vidal, K. Kifßner, L. Hammer, M. A. Schneider, T. Fauster, G. Sangiovanni, D. Di Sante, and F. Reinert, *Orbital-Driven Rashba Effect in a Binary Honeycomb Monolayer  $AgTe$* , Phys. Rev. Lett. **124**, 176401 (2020).
- [37] N. Reyren, S. Thiel, A. D. Caviglia, L. Fitting Kourkoutis, G. Hammerl, C. Richter, C. W. Schneider, T. Kopp, A.-S. Rüetschi, D. Jaccard, M. Gabay, D. A. Muller, J.-M. Triscone, J. Mannhart, *Superconducting Interfaces Between Insulating Oxides*, Science **317**, 1196 (2007).
- [38] A. D. Caviglia, S. Gariglio, N. Reyren, D. Jaccard, T. Schneider, M. Gabay, S. Thiel, G. Hammerl, J. Mannhart, J.-M. Triscone, *Electric field control of the  $LaAlO_3/SrTiO_3$  interface ground state*, Nature **456**, 624 (2008).
- [39] G. De Simoni, F. Paolucci, P. Solinas, E. Strambini, and F. Giazotto, *Metallic supercurrent field-effect transistor*. Nat. Nano. **13**, 802 (2018).